

Deep Reinforcement Learning for Orchestrating Cost-Aware Reconfigurations of vRANs

Fahri Wisnu Murti, Samad Ali, George Iosifidis, Matti Latva-aho

Abstract

Virtualized Radio Access Networks (vRANs) are fully configurable and can be implemented at low cost over commodity platforms offering unprecedented network management flexibility. However, their deployment faces complex configuration options, which leads to previously-unseen management challenges. In this paper, a novel deep Reinforcement Learning (RL)-based framework is proposed that jointly reconfigures the functional splits of the Base Stations (BSs), resources and locations of the virtualized Central Units (vCUs) and Distributed Units (vDUs), and the routing for each BS data flow. The objective is to minimize the long-term total network operation cost while adapting to the possibly-varying traffic demands and resource availability. To achieve this, in the first step, testbed measurements are performed to study the relations between traffic demands and computing resource utilization, which reveal that their relations have high variance and dependence on platform and platform load. Hence, acquiring the perfect model of the underlying vRAN system is highly non-trivial. A comprehensive cost function is also formulated that considers resource overprovisioning, instantiation and reconfiguration and the declined demands, where such impacts urge to perform the reconfigurations prudently. Motivated by these insights, our solution framework is developed using model-free multi-agent RL, where each agent controls the configurations of each BS. However, each agent has a multi-dimensional discrete action space due to the joint configuration decision of the BS, which drives combinatorial growth of the number of possible actions. In order to overcome the curse of dimensionality, incorporation of Dueling Double Q-network (Dueling DDQN) with action branching, a shared decision module followed by neural network branches, is applied at each agent to reduce the number of estimated actions drastically. Further, the agent learns its optimal policy to select an action that reconfigures the BS independently. Simulations are performed using O-RAN compliant model and real traces collected from the testbed. Our numerical results show that the proposed framework successfully learns the optimal policy and can be readily applied to different vRAN systems via transfer learning, which facilitates its widespread deployment and faster learning convergence. It also achieves significant cost savings by up to 45% of the static benchmarks and 33% of a non-branching Dueling DDQN solution.

I. INTRODUCTION

Virtualization has become one of the most promising technologies for accommodating the increased service demands with diverse requirements at a reasonable cost in cellular networks [1]. The latest effort of this idea is virtualizing the Radio Access Networks (vRANs) by replacing the hardware-based legacy RANs with softwarized RANs [2]–[4]. Incorporated with

Fahri Wisnu Murti, Samad Ali and Matti Latva-aho are with Centre for Wireless Communications, University of Oulu, Finland. George Iosifidis is with Delft University of Technology, Netherlands.

This research has been supported by the Academy of Finland, 6G Flagship program under Grant 346208. The work of G. Iosifidis has been supported by the European Commission through Grant No. 101017109 (DAEMON project).

Open RAN, vRANs can be fully configurable and deployed across heterogeneous platforms such as commodity servers and small embedded devices. Another exciting feature of vRANs is that it enables the baseband functions (BBU) of each Base Station (BS) to be disaggregated, hosted at the virtualized Distributed Units (vDUs) and Central Units (vCUs), and executed as Virtual Machine (VM) instances or light-weight containers over geo-distributed locations. This paradigm shift brings unprecedented flexibility to RAN operations, mitigates vendor lock-in, offers fast deployment and potentially reduces operational expenses [4]. Therefore, it is not surprising that many standardization bodies envision the virtualization for their future RANs, such as O-RAN [5] and 5G+ RAN [6].

Nevertheless, the expansive deployment of vRANs is still hindered by complex configuration options, which introduce new network management challenges in deploying cost-efficient vRAN configurations while serving the traffic demands. In particular, the operators need to decide the *functional splits* of the BSs to determine which BS functions are deployed at the vDUs and which are at the vCUs. Each choice of these splits has a different delay requirement, consumes different computing resources for the vDUs/vCUs, and generates a different data load over the xHaul links¹. Moreover, the vDUs/vCUs are executed on top of commodity platforms as VM instances or containers; hence, the operators need to allocate the *virtualized resources* (e.g., CPUs, memory) for them. There are also several candidate deployment locations for each vDU/vCU, possibly with different hosting machines, and this creates the *placement problem* in determining their optimal locations and platforms. At the same time, each placement location is associated with different eligible *routing paths* to transfer the data flow of the BSs, which incur particular delays and costs. Consequently, these issues create a challenging coupling among the BS splits, placement and allocated resources for the vDUs/vCUs, and routing for each BS data flow.

Meanwhile, the suitability of the vRAN configurations is highly affected by the network properties such as traffic demands and resource availability (e.g., computing and xHaul link capacity) [7], which might change over time, often in an unpredictable fashion². Thus, deploying static configurations for a long time might result in resource overprovisioning or even declined

¹The paths connecting a core network (EPC) to vCUs, vCUs to vDUs, and vDUs to Radio Units (RUs) are defined as backhaul (BH), midhaul (MH), fronthaul (FH), respectively, and the integration of these elements is called Crosshaul/xHaul transport network.

²This is particularly common for resource availability/costs in shared infrastructures or traffic and channel conditions in small cell networks [8].

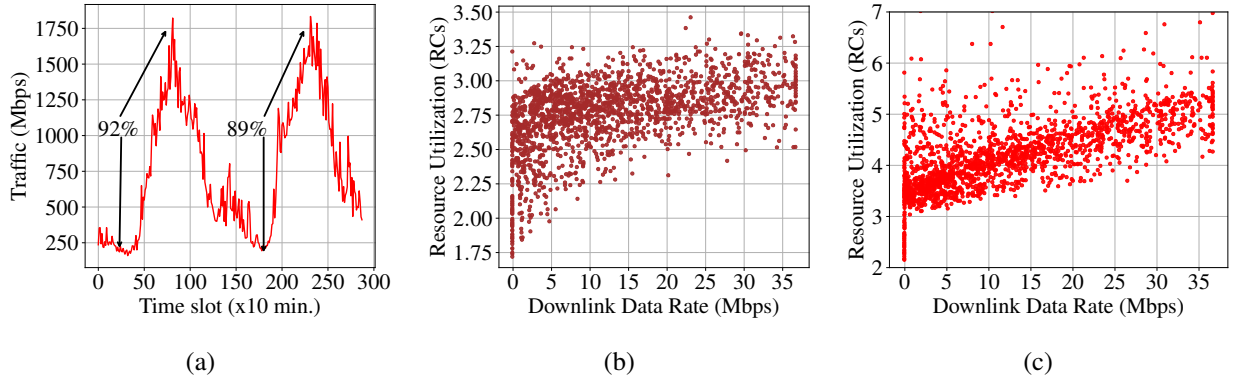


Fig. 1: **a)** Traffic variation within two days from Milan datasets [12] and **b)** collected measurement results over Platform A and **c)** Platform B. The resource utilization is presented in a reference core (RC), which translates to 1 virtual CPU/thread. The detailed experiment setups and datasets are presented in Sec. IV.

traffic demands. Resource overprovisioning occurs when the allocated resources are higher than the actual resource utilization. The declined demands can be triggered by insufficient allocated resources (underprovisioning) and constraint violation. And these can render substantial performance degradation and high operating expenditures. Therefore, it is essential to dynamically select the vRAN configurations to adapt to varying traffic demands and resource availability.

On the other hand, orchestrating the dynamic configurations of vRANs is a non-trivial endeavor. The reconfiguration decisions must be enforced before the actual traffic demands of the BSs are observed. Albeit reconfiguring the vRAN system at runtime is practically possible [9], it might also induce additional costs and disrupt network operations during the live migration of the VM instances. Consequently, any reconfiguration activity needs to be performed prudently to ensure that it is beneficial both in terms of cost and performance. However, designing such an intelligent approach also has technical issues since the software-based vRAN system substantially differs from hardware-based legacy RANs. The takeaway from our testbed measurements (see Fig. 1) and prior experimental studies (cf., [10], [11]) is that, unlike legacy RANs, the underlying system of vRANs is complex, poly-parametric and has platform-dependent performance. Hence, adopting traditional control policies, which needs perfect knowledge of the underlying system to model and solve the problems, is unrealistic in practice.

Measurement insights. Fig. 1a illustrates an example of the traffic demand of a BS in the Milan datasets [12]. It shows a significant difference between the peak and lowest traffic demand by up to 92% in a single day. Moreover, the traffic variation might vary from day to day (e.g., weekdays, weekends). Figs. 1b and 1c show that the traffic demand highly affects the resource utilization of the BBU. These findings motivate us to implement the dynamic configurations to

adapt such traffic and resource variations to achieve cost-effective operations. Figs. 1b and 1c also demonstrate that the relations between traffic demand and resource utilization have high variance, where we found a significant degree of spread on the resource utilization. Moreover, these relations are platform-dependent performance (e.g., hanging on the hosting platforms and platform load). For example, although they indicate not strongly linear in Platform A and B, the resulting Pearson coefficient is different with 0.513 and 0.654, respectively. Also, albeit the BBU has been reserved with the same resources, Fig. 1c shows that the BBU utilization of Platform B is higher than Platform A. Such platform-dependent performance is also found in [10] for uplink, where the computing behavior of vRANs is identified depending on many latent factors.

The above issues and insights motivate us to develop a novel intelligent framework based on Machine Learning (ML) in order to tackle the reconfiguration problem in vRANs with minimal assumptions about the system.

A. Related Work

Recent works have studied optimizing various vRAN configuration options to achieve a cost-efficient deployment, such as their integration with Mobile Edge Computing (MEC) [13] and interoperability with Open RAN [14]. However, these works aimed at offline network design and did not study the implication of varying conditions from traffic demands and resource availability. Recent studies have considered dynamically altering the vRAN configurations at runtime to maximize the users' throughput [15] and revenue [16] and to minimize the inter-cell interference and FH utilization [17]. However, they focused on reconfiguring the functional splits. We argue that the other vRAN configurations, such as the allocated resources of the vDUs and vCUs and their placement, are also crucial to be reconfigured. Moreover, the mentioned works [13]–[17] indeed have solved various vRAN problems, but they utilized mathematical tools that require perfect knowledge of the underlying system and relied on fine-tune models for specific scenarios. In marked contrast, our framework is developed based on a model-free learning algorithm and makes minimal assumptions about the system.

ML techniques have been increasingly popular to tackle complex problems in wireless networks, offering satisfactory performance while making minimal assumptions about the underlying system [18]. In vRANs, the authors in [10] have tailored a deep learning-based framework to solve the contextual bandit problem of managing the interplay between computing and radio resources. Then, their follow-up work [11] utilizes Bayesian online learning for

balancing performance and energy consumption. Recent works in [19], [20] have brought the importance of Reinforcement Learning (RL) to optimize the split selections. The authors in [21] and their follow-up study [22] have developed xApps for RL-based controls of RAN slicing, scheduling and online model training, including their implementation in O-RAN compliant experimental platforms. Indeed, these works have successfully solved complex optimization and control problems in vRANs. However, they did not study the effects of reconfiguring the allocated resources and locations of the vCUs/vDUs at runtime. Our recent work [23] has shown the importance of such effects and proposed an RL-based framework using a combination of Deep Q-Network (DQN) and a regressor to minimize the long-term operation cost. However, it only explored a joint decision between the split and resources and was limited to a single BS. Here, we examine a fresh vRAN reconfiguration problem by considering a vRAN system with multiple BSs that jointly reconfigure the splits of the BSs, resources and locations of the vDUs and vCUs, and the routing of each BS data flow. To the best authors' knowledge, this problem is hitherto unexplored and drives the prior vRAN frameworks not applicable. To this end, we also develop a novel framework to solve this new reconfiguration problem.

B. Contributions and Methodology

The main contribution of this paper lies in a novel learning-based automated reconfiguration framework (LARV) that tackles the reconfiguration problem of vRANs. LARV jointly reconfigures the splits of the BSs, the resources and locations of the vDUs and vCUs over geo-distributed platforms, and the routing for each BS data flow. The objective is to build cost-efficient and economically sustainable operations by minimizing the long-term total operation cost.

In particular, we firstly build a prototype implementing the Centralized-RAN (C-RAN) system using software-based srsRAN [24] in two different platforms to collect measurements regarding the relations between traffic demands and resource utilization. The findings reveal that the relations vary with the demands and, importantly, have high variance and dependence on the platform, platform load, and many latent factors. These inhibit adopting general assumptions of the underlying system (e.g., linear) and traditional mathematical tool-based policies. Then, we propose a new cost model accounting for resource overprovisioning, instantiation and reconfiguration and the declined traffic demands, representing the virtualized resource management in vRANs. This model also considers different computing and routing costs for each split and platform location. Further, we model our vRAN system following the latest proposal of O-RAN

architecture [5]. We consider a vRAN system with multiple BSs and define its operation as a time-slotted system, where each slot has arbitrary incoming traffic demands and resource availability. At each time slot, LARV decides whether to preserve the previous network configurations or reconfigure them. This sequential decision-making problem is formulated as generalization of the Markov Decision Process (MDP) or Markov games.

In our solution, LARV is developed using model-free Multi-Agent RL (MARL) with neural network architecture, where each agent controls the reconfigurations of each BS. Each agent learns its optimal policy to select an action that reconfigures the BS non-cooperatively via independent learning (IL) by considering the other agents as part of its environment. This paradigm demonstrates a linear increase in the agents' action spaces with the number of BSs instead of combinatorial growth. Moreover, the agents do not need to make any particular assumptions about the underlying system state and state transition probability distribution. They also do not need to exchange learning information as there is no coordination; hence, computational and communication burdens can be substantially reduced. Besides, LARV can be readily tailored to a single agent case, i.e., a vRAN system with a single BS. However, each agent has a multi-dimensional and large discrete action space due to the joint decision between the split, resource, location, and routing at each BS; and this renders combinatorial growth of the neural network's output. To overcome the curse dimensionality, we incorporate action branching [25], a shared decision module followed by neural network branches, with Dueling Double Q-network (Dueling DDQN) [26] for each agent's neural network architecture called BDQ. As a result, at each agent, LARV exhibits a linear growth of the total neural network outputs with the increase of action dimensionality while maintaining the shared decision.

In our evaluations, we conduct a battery of tests using an O-RAN compliant model and real traces collected from the testbed. We evaluate the training behavior and accumulated total network operation cost during online operation under various scenarios. Our numerical results reveal that LARV successfully learns the optimal policy to select actions that reconfigure the BSs and can be readily adopted over different vRAN systems via transfer learning, which facilitates its widespread deployment and faster learning convergence. LARV also renders considerable cost savings by up to 45% of the static benchmarks and 33% of a non-branching Dueling DDQN solution. Our contributions can be summarized as follows:

- We propose and study a new vRAN reconfiguration problem, where it jointly reconfigures splits of the BSs, resources and locations of the vDUs/vCUs, routing for each BS flow.

- We carefully model our vRAN system based on the latest proposals of O-RAN architecture and propose a comprehensive cost model. The model takes resource overprovisioning, instantiation and reconfiguration and the declined demands costs into account. It also captures platform/split-dependent computing and routing costs.
- We develop a novel learning-based framework to solve our vRAN reconfiguration problem. It is tailored from MARL and BDQ architecture to tackle the multi-dimensional and large action space inherited from our RL problem with linear growth of the neural network output.
- We conduct extensive trace-driven simulations and analyze the performance of LARV under various scenarios during the training process and online operation.

The rest of this paper is organized as follows. In Sec. II, the architecture background and model used for our vRAN system are presented. The trade-offs and problem statements raised in our vRAN reconfiguration problem are also discussed in this section. Then, our problem is formulated as a generalized MDP in Sec. III, including how we design LARV as the solution framework. The detailed experiment setups and simulation results are presented in Sec. IV. Finally, our paper is concluded in Sec. V.

II. SYSTEM MODEL AND PROBLEM STATEMENT

A. O-RAN Background

We model our vRAN system following the latest proposals of O-RAN architecture [5], which also have envisioned learning-based orchestration for controlling the BS operations [21]. Each BS's protocol stacks (or functions) are disaggregated through the functional split and can be hosted at the vCU, vDU and RU. Hence, a BS corresponds to 4G eNodeB or 5G gNodeB comprising a vCU and a vDU connected to an RU. The vCU and vDU can be executed as VM instances or containers across geo-distributed edge cloud infrastructures. Then, LARV is to be implemented in the Learning Agent (LA) inside the Non-Real-Time (Non-RT) Intelligent Controller (RIC) in the system orchestrator of O-RAN. LARV enforces a policy at every period of $n=1, \dots, N$ to control the reconfigurations of BSs. Then, the optimal policy at every time n depends on the input observation (state), which is provided at the beginning of each period by the BSs through the O1 interface from the collected data measurements inside the Near-RT RIC (via E2 interface). A reward signal is computed at the Data Monitor module (inside Near-RT RIC) on each period. Fig. 2 shows the high-level architecture of our vRAN system.

Functional Splits. Fig. 3 illustrates the split options used in our model and Table I summarizes the splits and their requirements following 3GPP nomenclature [6]. We consider Option 7.x (O7)

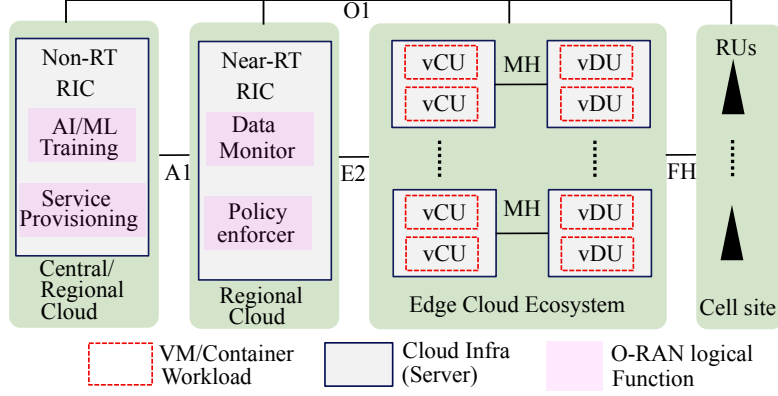


Fig. 2: O-RAN compliant system architecture adopted in our model.

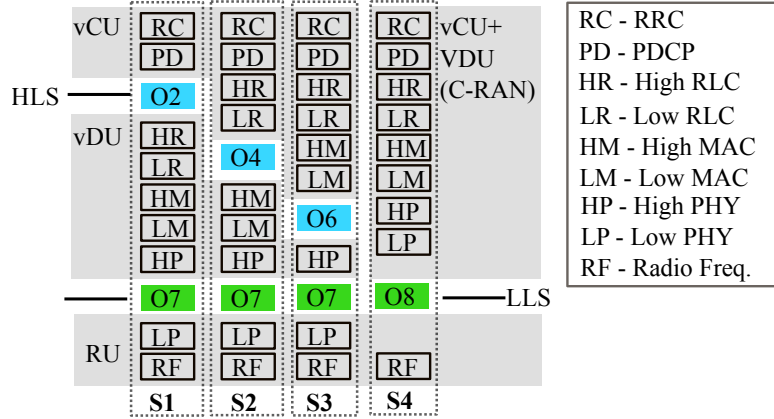


Fig. 3: The functional splits applied in our vRAN model. S1, S2 and S3 are envisioned in O-RAN architecture proposals, while S4 are legacy C-RAN.

and Option 8 (O8) for the Low Layer Split (LLS) between the vDU and RU. The High Layer Split (HLS) between the vCU and vDU can use Option 2 (O2), Option 4 (O4) and Option 6 (O6). These options are selected as they have been well standardized [5], [6] and experimentally validated [15]. Following HLS and LLS splits, we denote four choices of functional splits: *Split 1 (S1)* implements O2 for the HLS and O7 for the LLS; *Split 2 (S2)* uses O4 for the HLS and O7 for the LLS; *Split 3 (S3)* adopts O6 for the HLS and O7 for the LLS; and *Split 4 (S4)* is the legacy C-RAN system, which implements Option 8 (O8), i.e., all the BS functions are executed as an integrated vDU/vCU except RF functions (at the RU). We define a set of possible splits for S1, S2, S3 and S4 as $\mathcal{I} = \{S1, S2, S3, S4\}$.

B. Model

Network. The key notations are summarized in Table II. We consider a vRAN system with K BSs, where the functions of each BS- k can be disaggregated and hosted at vCU- k , vDU- k

Options	Split Point	Data Load	Max Load	Delay Req.
O1	RRC - PDCP	λ	4	10 ms
O2*	PDCP - High RLC	λ	4	10 ms
O3	High RLC - Low RLC	λ	4	10 ms
O4*	Low RLC - High MAC	λ	4	1 ms
O5	High MAC - Low MAC	λ	4	1 ms
O6*	Low MAC - High PHY	$1.02\lambda+0.5$	4.13	0.25 ms
O7 [†]	High PHY - Low PHY	10.1	10.1	0.25 ms
O8 [†]	Low PHY - RF	157.3	157.3	0.25 ms

Note: * is applied options for HLS and [†] is applied options for LLS. The data load is in Gbps.

TABLE I: The functional split options and their requirements based on 3GPP nomenclature when the traffic demand is λ Gbps. The requirements are tailored by following settings: 100 MHz bandwidth, 256 QAM, 32 antenna ports and 8 MIMO layers. The achievable data rate is up to 4 Gbps.

Descriptions	Notations
The traffic demand (split) of BS- k	λ_k^n (i_k^n)
Allocated flavors (actual resource utilization) for vDU- k /vCU- k	x_k^n/y_k^n (\hat{x}_k^n/\hat{y}_k^n)
Locations of vDU- k and vCU- k	z_k^n, ζ_k^n
Maximum computing capacity of FS- l and ES- m	H_l, \hat{H}_m
A connecting path of EPC \rightarrow ES- m , ES- $m\rightarrow$ FS- l , ES- $m\rightarrow$ RU- k , FS- $l\rightarrow$ RU- k	$p_{0m}, p_{ml}, p_{mk}, p_{lk}$
Incurring delay of path $p_{0m}, p_{ml}, p_{mk}, p_{lk}$	$d_{p_{0m}}, d_{p_{ml}}, d_{p_{mk}}, d_{p_{lk}}$
HLS and LLS delay requirement for split i	d_i^H, d_i^L
The routing for BS- k	$p \in \mathcal{P}_k$
Data flow with split i via routing $p \in \mathcal{P}_k$ (FH, MH, BH)	$(r_{p,i}^{FH,n}, r_{p,i}^{MH,n}, r_{p,i}^{BH,n})$

TABLE II: Key variables and parameters used in our model.

and RU- k . The vDUs are executed at far-edge cloud servers (FSs) while the vCUs are at edge cloud servers (ESs)³. We model a packet-based vRAN as a graph of $G = (\mathcal{V}, \mathcal{E})$, where the set of physical nodes \mathcal{V} includes the subsets: $\mathcal{K} = \{1, \dots, K\}$ of RUs, $\mathcal{L} = \{1, \dots, L\}$ of FSs, $\mathcal{M} = \{1, \dots, M\}$ of ESs, EPC (index 0), and routers. These nodes are connected through a set of links \mathcal{E} , where each link $(i, j) \in \mathcal{E}$ has a data transfer capacity c_{ij} (Gbps). We denote \mathcal{P}_k as a set of paths connecting EPC to RU- k and consider the data flow for each BS is unsplittable. We focus on the downlink, but it is not limited and can easily be extended for uplink. The data flow for

³FSs are the candidate platforms and locations to execute VM instances of the vDUs. Similarly, ESs are the candidate platforms and locations for the vCUs. We also consider ESs for the candidate platforms to host an integrated vDU/vCU in C-RAN. ESs are typically located at more centralized locations, while FSs are co-located or near the RUs.

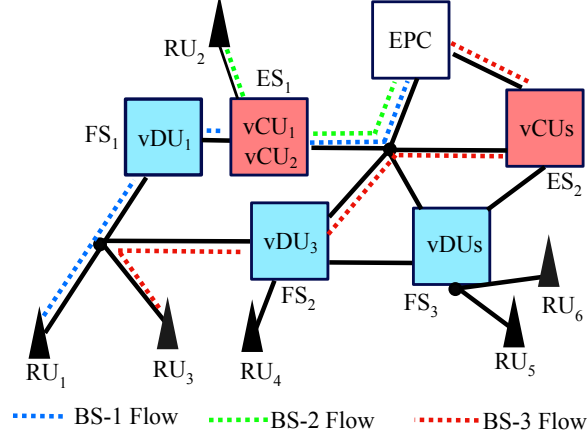


Fig. 4: The functions of each BS can be split between the vCU, vDU and RU. For BS-1, vDU-1 and vCU-1 are executed at FS-1 and ES-1, respectively. However, BS-2 implements C-RAN (S4); hence, the integrated vDU/vCU are executed only at ES-1 (e.g., links to and instances at FSs are not activated). Then, vDU-3 and vCU-3 of BS-3 are hosted at FS-2 and ES-2, respectively.

each BS will be transferred from EPC to RU- k through a path $p := \{(0, i_1), (i_1, i_2), \dots, (i_k, k) : (i, j) \in \mathcal{E}\} \in \mathcal{P}_k$. Since this path might pass through FSs and ESs before reaching each RU, let us denote p_{0m} , p_{ml} , p_{mk} , and p_{lk} as a path connecting $\text{EPC} \rightarrow \text{ES-}m$, $\text{ES-}m \rightarrow \text{FS-}l$, $\text{ES-}m \rightarrow \text{RU-}k$, and $\text{FS-}l \rightarrow \text{RU-}k$, respectively. Based on the selected split, the data flow of each BS- k passes through $p := p_{0m} \cup p_{ml} \cup p_{lk} \in \mathcal{P}_k$ ($\text{EPC} \rightarrow \text{ES-}m \rightarrow \text{FS-}l \rightarrow \text{RU-}k$) if activating S1, S2 and S3. Otherwise (e.g., S4/C-RAN), the flow passes through $p := p_{0m} \cup p_{mk} \in \mathcal{P}_k$ ($\text{EPC} \rightarrow \text{ES-}m \rightarrow \text{RU-}k$ without using FSs). Each path has a total delay defined as d_p , $d_{p_{0m}}$, $d_{p_{ml}}$, $d_{p_{mk}}$ and $d_{p_{lk}}$; and they must respect the delay requirements of the split as described in Table I. We compute each p_{0m} , p_{ml} , p_{mk} and p_{lk} with the shortest path method [27]. Fig. 4 shows an example of our model.

Platforms & Resources. We use the term *flavor*⁴ to define the available choices for allocating the virtualized computing resources. Let us introduce \mathcal{X} as a set of available flavors for the vDUs and vCUs. Then, we select a flavor $x_k \in \mathcal{X}$ and $y_k \in \mathcal{X}$ that directly determine the reserved resources for each vDU- k (in FSs) and vCU- k (in ESs), respectively. Each FS- l has physical computing capacity H_l , respectively \hat{H}_m for ES- m , which bound the aggregate allocated resources (accordingly, the flavors that can be selected) of the vDUs and vCUs for each location.

⁴This term is carried out from OpenStack (<https://www.openstack.org/>) to reserve the amount of virtual CPU, memory, and storage capacity for a VM instance. This term is typically used to calculate the billing units to charge the amount of monetary cost. Similar terms are also used in other cloud services such as AWS and Azure. Here, we focus on the CPU resources as they are the most affected performance by the traffic demands.

Reconfiguration controls. We model the vRAN operation as a time-slotted system, where each slot has possibly-different incoming traffic demands and resource availability. The incoming traffic of BS- k at time slot n is denoted as $\lambda_k^n \geq 0$ (Gbps). At each time slot n , the operators can choose to reconfigure **(i)** the functional splits $i_k^n \in \mathcal{I}, \forall k \in \mathcal{K}$; **(ii)** the flavors to allocate virtualized resources for the vDUs $x_k^n \in \mathcal{X}, \forall k \in \mathcal{K}$ and **(iii)** vCUs $y_k^n \in \mathcal{Y}, \forall k \in \mathcal{K}$; **(iv)** the locations of vDUs over FSs $z_k^n \in \mathcal{L}, \forall k \in \mathcal{K}$ and **(v)** vCUs over ESs $\zeta_k^n \in \mathcal{M}, \forall k \in \mathcal{K}$; and **(vi)** the routing paths $p^n \in \mathcal{P}_k, \forall k \in \mathcal{K}$. Otherwise, they can choose not to reconfigure the system by preserving their last network configurations.

C. Source of monetary costs and objective

In our evaluation, the source of monetary costs comes from the computing cost to execute the BS functions, the virtualized resource management costs and the routing cost.

Computing costs. The needs of computing cost of each BS- k to host its functions at the RU- k , vDU- k (in the FS) and vCU- k (in the ES) are denoted as:

$$f_{\text{RU}}(\hat{w}_k^n), f_{\text{FS}}(\hat{x}_k^n), \text{ and } f_{\text{ES}}(\hat{y}_k^n), \quad (1)$$

where $f_{\text{RU}}(\cdot)$, $f_{\text{FS}}(\cdot)$ and $f_{\text{ES}}(\cdot)$ are the cost functions to charge the utilized computing processing at the RU⁵, FS and ES, respectively. These cost functions translate the actual computing resource utilization of RU- k $\hat{w}_k^n \in \mathbb{R}$, vDU- k $\hat{x}_k^n \in \mathbb{R}$ and vCU- k $\hat{y}_k^n \in \mathbb{R}$ into monetary units (\$). The actual resource utilization of RU, vDU and vCU are highly affected by the split and demand at the BS. Hence, we define $\psi : (\lambda_k^n, i_k^n) \mapsto (\hat{w}_k^n, \hat{x}_k^n, \hat{y}_k^n)$ as a function to map inputs of the split and traffic demand of the BS into the actual resource utilization at the RU, vDU and vCU. This function represents the actual computing behavior in the vRAN system, and we characterize it through traces from the testbed measurements. Further, we consider that cost functions $f_{\text{RU}}(\cdot)$, $f_{\text{FS}}(\cdot)$ and $f_{\text{ES}}(\cdot)$ to be proportional with their input, e.g., $f_{\text{FS}}(v) := \kappa_{\text{RU}}v$, $f_{\text{FS}}(v) := \kappa_{\text{FS}}v$ and $f_{\text{ES}}(v) := \kappa_{\text{ES}}v$, where κ_{RU} (\$/unit), κ_{FS} (\$/unit) and κ_{ES} (\$/unit) are the estimated computing processing fees per core unit capacity at the RUs, FSs and ESs, respectively.

Resource Management Costs. In vRANs, the vDUs and vCUs are virtualized on the FSs and ESs, respectively. Therefore, the virtualized resources of the vDUs and vCUs can be dynamically allocated to obtain cost-efficient network operations. However, reconfiguring such resources

⁵RUs are the radio hardware units; hence we do not allocate resources for RU. Instead, the computing cost of the RUs is incurred from processing the LP/RF functions, where their processing cost is demand/split dependent.

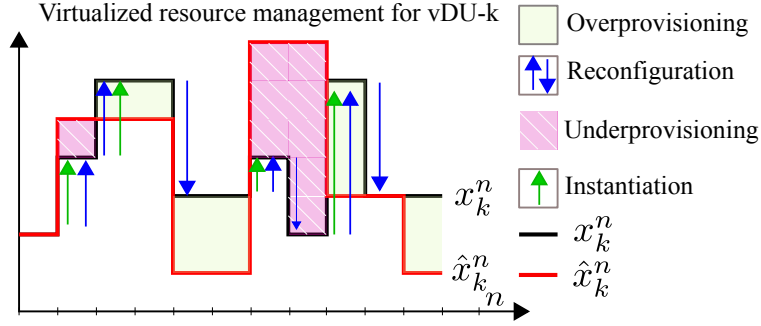


Fig. 5: An example of virtualized resource management model for vDU- k .

might create to additional costs. Meanwhile, the allocated resources x_k^n and y_k^n might differ to the actual resource utilization of \hat{x}_k^n and \hat{y}_k^n , which can create to unwanted resource overprovisioning or declined demands. Motivated by resource management in network slicing [28], we propose a cost model capturing such behaviors in vRANs. This model is illustrated in Fig. 5 and described as follows.

(i) Overprovisioning: If the allocated resources are higher than their actual utilization, the operators pay more expenses and miss the opportunity to share their unused resources for other workloads. Such resources are instantiated and reserved for no purpose, which can be more profitable to be allocated for other workloads (e.g., video analytics) to increase the global system efficiency. This overprovisioning cost at time slot n is defined as:

$$f_O(\max(0, x_k^n - \hat{x}_k^n) + \max(0, y_k^n - \hat{y}_k^n)), \quad (2)$$

where $f_O(\cdot)$ is a cost function for resource overprovisioning. This function is proportional with the input, e.g. $f_O(v) := \kappa_O v$, where κ_O is the estimated fee for one unit capacity (\$/unit).

(ii) Declined service demands: The declined demands can occur when there exists an insufficient resource allocation or constraint violation, which triggers service level agreement (SLA) violation and monetary compensation. For instance, the constraint violation can happen when the total allocated resources of the vDUs exceed FS capacity:

$$f_D\left(\max\left(0, \sum_{k \in \mathcal{K}} x_k^n \mathbb{1}_{=l}(z_k^n) - H_l\right)\right), \quad \forall l \in \mathcal{L}, \quad (3)$$

the total allocated resources of the vCUs exceed ES capacity:

$$f_D\left(\max\left(0, \sum_{k \in \mathcal{K}} y_k^n \mathbb{1}_{=m}(\zeta_k^n) - \hat{H}_m\right)\right), \quad \forall m \in \mathcal{M}, \quad (4)$$

and the incurred delay does not meet the requirement:

$$f_D(\max(0, d_{p_{ml}} - d_i^H, d_{p_{lk}} - d_i^L, d_{p_{mk}} - 0.25)), \quad \forall m \in \mathcal{M}, \quad \forall l \in \mathcal{L}, \quad (5)$$

where d_i^H and d_i^L are the delay requirement of split i for the HLS and LLS, respectively, as defined in Table I. In addition to the constraint violation, an insufficient allocation for each vDU and vCU can cause declined service demands, and we define this as:

$$f_D(\max(0, \hat{x}_k^n - x_k^n, \hat{y}_k^n - y_k^n)). \quad (6)$$

The function $f_D(\cdot)$ captures the monetary compensation that the operators have to pay for violating the SLA. This function is assumed to be proportional with the input, e.g. $f_D(v) := \kappa_D v$, where κ_D is the estimated fee for declined demands in one unit capacity (\$/unit).

(iii) Instantiation and Reconfiguration: The operators may decide to instantiate new resources or reconfigure their network settings to reduce resource overprovisioning and declined demands and adapt to the varying traffic demands and resource availability. However, instantiating and reconfiguring such resources (e.g., VMs) induce capital expenses, and we define it as:

$$f_I(\max(0, x_k^n - x_k^{n-1}) + \max(0, y_k^n - y_k^{n-1})), \quad (7)$$

$$f_R\left(\left(|x_k^n - x_k^{n-1}| + |y_k^n - y_k^{n-1}|\right) + \left(x_k^n \mathbb{1}_{\neq z_k^{n-1}}(z_k^n) + y_k^n \mathbb{1}_{\neq \zeta_k^{n-1}}(\zeta_k^n)\right)\right), \quad (8)$$

where $f_i(\cdot)$ and $f_r(\cdot)$ are the cost functions for resource instantiation and reconfiguration.

Eq. (7) captures the amount of instantiating additional resources for the vDU and vCU, which might arise due to migrating additional resources to serve the vRAN workload, and this results in indirect overhead expenses such as the increase of power consumption [28]. Then, the first term in (8) captures the reconfiguration cost initiated from migration activities for altering the splits and flavors (resizing resources). Such activities raise overhead costs from the migrated resources, measured from the difference between the current and the previous resources [9], [28]. For instance, altering the splits requires creating new BS functions while maintaining the old migrated functions to keep active [9]. Resizing the VMs' resources also initiates a price of management delay [29] as it needs time for migrating (and bootstrapping) the computing resources, load balancing and steering the network load⁶. The second term in (8) captures the reconfiguration cost for migrating the vDU and vCU instances to other FS and ES locations. In this case, the whole resources of vDU and vCU instances are affected, and the attached routing paths need to be recomputed with the new FS and ES locations. In our evaluation, $f_i(\cdot)$ and

⁶We have calculated the incurred time for resizing a VM instance in CSC cPouta (<https://www.csc.fi/>) cloud computing platform, and it takes around 25 seconds. Modern software architecture such as Kubernetes also requires several seconds to executing new pods [28].

$f_R(\cdot)$ are proportional to the input, e.g., $f_I(v) := \kappa_I v$ and $f_R(v) := \kappa_R v$, where κ_I (\$/unit) is the estimated cost for resource instantiation and κ_R (\$/unit) is for reconfiguration. If reconfiguring the system do not incur any overhead cost, we can set $\kappa_R = 0$, otherwise $\kappa_R > 0$.

Routing Cost. O-RAN has encouraged adopting an open interface between the vCUs, vDUs and RUs [5], resulting in sharing the xHaul links among the BSs. In addition, S1, S2, S3 and S4 generate different data loads depending on the selected split as seen in Table I. Hence, the cost for reserving bandwidth and routing the data flow through the xHaul links are also different. The routing cost for each BS- k can be denoted as:

$$f_H \left(\sum_{p \in \mathcal{P}_k} \left(r_{p,i}^{\text{FH},n} \sum_{l \in \mathcal{L}} \mathbb{1}_{=z_k^n}(l) + r_{p,i}^{\text{MH},n} \sum_{m \in \mathcal{M}} \mathbb{1}_{=\zeta_k^n}(m) + r_{p,i}^{\text{BH},n} \right) \right), \quad (9)$$

where $r_{p,i}^{\text{FH},n}$, $r_{p,i}^{\text{MH},n}$, $r_{p,i}^{\text{BH},n}$ are the incurred data loads over FH, MH and BH at time slot n from using path p , serving traffic demand λ , and deploying split- i . The indicator $\mathbb{1}_{=z_k^n}(l)$ activates if vDU- k is placed at FS- l and $\mathbb{1}_{=\zeta_k^n}(m)$ activates if vCU- k is hosted at ES- m . Then, $f_H(\cdot)$ is the cost function for bandwidth reservation to transfer data load through the xHaul links, and this cost function is proportional with the input, e.g., $f_H(v) := \kappa_H^p v$, where κ_H^p (\$/Gbps/Km) is the estimated fee for reserving bandwidth for path p per Gbps/Km.

Objective. We aim to minimize the accumulated total network operation cost over period of time. The source of monetary costs are accounted from (1)-(9). Let suppose $J_k^n := f_{\text{RU}}(\cdot) + f_{\text{FS}}(\cdot) + f_{\text{ES}}(\cdot) + f_{\text{O}}(\cdot) + f_{\text{D}}(\cdot) + f_{\text{I}}(\cdot) + f_{\text{R}}(\cdot) + f_{\text{H}}(\cdot)$ is the operation cost for each BS- k at time slot n . The total operation cost per time slot for all the BSs can be defined as $J^n := \sum_{k \in \mathcal{K}} J_k^n$. Then, our goal is to design *an optimal joint policy* (π_*) that decides the BS splits, flavors and locations of the vDUs and vCUs, and the routing of each BS flow to minimize the long-term accumulated total operation cost:

$$\pi_* := \arg \min_{\pi} \mathbb{E}_{\pi} \left[\sum_{\tau=0}^{\infty} \gamma^{\tau} J^{\tau+n} | \pi \right], \quad (10)$$

where $\mathbb{E} \left[\sum_{\tau=0}^{\infty} \gamma^{\tau} J^{\tau+n} \right]$ is the expected long-term accumulated total operation cost starting at time slot τ , $\gamma \in (0, 1]$ is the discount factor, and $\pi = \{\pi_1, \dots, \pi_K\}$ is the joint policy of the BSs.

D. Trade-offs and Problem Statement

The above sequential decision problem is intricate for many reasons. We provide the trade-offs and non-triviality that arise as follow.

(i) From S1 to S4, the operators can gain a lower computational cost and high-performance operations through function centralization. However, it also has a tighter constraint requirement

and induces a higher transferred data load through the xHaul links. A higher data load means a more expensive routing cost. In addition to the splits, the required resources for the vDUs and vCUs are highly affected by traffic demand and resource availability, which might change absurdly. These also affect the placement of the vDUs and vCUs over FSs and ESs. The association and routing paths are also different for each placement location.

(iii) Using a static policy and finding the best configurations by foreseeing the future peak traffic may reduce the overhead costs due to reconfiguration activities. However, it might produce significant resource overprovisioning. Such unused resources can be profitable if the operators can efficiently manage and share with other workloads. Predicting the future peak traffic might also be inaccurate, which might not result in the best configurations.

(ii) By dynamically reconfiguring the vRAN settings at every time slot, the operators can obtain the best configurations at a time; hence, the risks of resource overprovisioning and declined demands can be reduced. However, every reconfiguration activity produces overhead costs, which may lead to costly long-term network operations. Moreover, the reconfiguration decisions are made before the actual traffic demand is observed; therefore, finding the optimal decisions at every time slot is challenging and might be unfeasible in practice.

(iv) The reconfiguration decisions in our vRAN system are highly affected by the traffic demands and resource utilization. However, their relations are complex, depending on many factors such as traffic demand, computing platform, radio scheduler, etc, which also hinder general assumptions (e.g., linear) to model the computing resource's behavior, rendering traditional control policies inefficient for our vRAN reconfiguration problem.

(v) Points (i)-(iv) emphasize the need for intelligent reconfiguration decisions with minimal assumptions about the underlying system. A deep RL paradigm can be suitable to handle such challenges. However, the action space inherited from our RL problem is multi-dimensional and extremely large, even for a single BS. Moreover, a vRAN system typically consists of multiple BSs that share the same network links and computing resources. These challenges make conventional deep RL discrete action space algorithms such as deep Q learning inefficient. In order to tackle these challenges, a novel algorithm design is necessary.

Problem statement. Given the above trade-offs, traffic demands, and resource availability, how to design a joint policy that intelligently reconfigures the splits of the BSs, the resources and locations of the vDUs and vCUs, and the association and routing for each BS flow, thus the long-term total network operation cost is minimized?

Next, we present how we formulate the above sequential decision-making problem and discuss how to design the solution approach that can solve the problem efficiently.

III. LARV SOLUTION DESIGN

A. MARL Problem Formulation

LARV adopts model-free MARL paradigm with BDQ architecture to solve the sequential decision-making problem defined in Sec. II. In particular, the problem is formulated as generalization of the MDP (Markov games), specified by a tuple $\{\mathcal{K}, \mathcal{S}, \mathcal{A}, \mathcal{P}, r, \gamma\}$, where:

- \mathcal{K} is the set of agents and $K = |\mathcal{K}|$ is the number of agents, where each agent controls the reconfiguration decisions of each BS;
- $\mathcal{S} = S_1 \times \dots \times S_K$ is the state space of the BSs in a vRAN system;
- $\mathcal{A} = A_1 \times \dots \times A_K$ is the joint action space of all the agents;
- $\mathcal{P} : \mathcal{S} \times \mathcal{A} \times \mathcal{S} \rightarrow [0, 1]$ is the state transition probability distribution, which depends on the actions of the agents; and
- $r = \{r_1, \dots, r_K\}$ is a set of real value rewards received by our agents from the environment.

LARV adopts a non-cooperative setting where the agents learn their optimal policy through IL. Each agent is selfish and rational, treats other agents as part of its environment, and only observes its own state and reward. Therefore, the agents do not perform any information exchange with each other (no coordination), and the agents' action spaces can be reduced to a linear increase with the number of BSs. As a result, LARV (by using IL) requires less storage, communication and computing overhead than the cooperative learning mechanism [30]. The decision problem faced by an agent when all the other agents use a fixed strategy profile is also equivalent to an MDP [31]. Hence, at every time slot n , each of our agents observes the locally information state from its local state space $s_k^n \in \mathcal{S}_k \subseteq \mathcal{S}$ drawn from the environment, takes an action from the locally action space $a_k^n \in \mathcal{A}_k \subseteq \mathcal{A}$, and expects to receive a reward signal $r_k(s_k^n, a_k^n)$ as a feedback. The state also may not be stationary as the traffic demands and network states are changing over time with the sequence state arrival $(s_k^n)_{n \in \mathcal{N}, k \in \mathcal{K}}$. Then, the state transition probability of agent k that maps a state-action pair at time step n into the distribution of next state is defined by $\mathcal{P}_k(s_k^{n+1} | s_k^n, a_k^n)$, and we take no assumption about it.

1) *State*: The state observation of each agent k consists of: (i) the incoming traffic demand λ_k^n , (ii) the previous deployed split i_k^{n-1} , (iii) the previous allocated resources (flavors) for the vDU x_k^{n-1} and (iv) vCU y_k^{n-1} , and (v) the previous deployed locations of vDU- k over FS z_k^{n-1}

and (v) vCU- k over ES ζ_k^{n-1} . It provides *time dynamic* of our variable interests: (i) the demand that needs to be served by each BS, (ii) the current active split, (iii) the availability of resources for the vDU and (iv) vCU; and (v) the availability to execute the vDU at FS and (vi) the vCU at ES. Then, the state observation of each BS- k at time slot n is denoted as:

$$s_k^n := \{\lambda_k^n, i_k^{n-1}, x_k^{n-1}, y_k^{n-1}, z_k^{n-1}, \zeta_k^{n-1}\} \in \mathcal{S}_k, \quad \mathcal{S}_k = \mathbb{R} \times \mathcal{I} \times \mathcal{X} \times \mathcal{X} \times \mathcal{L} \times \mathcal{M}. \quad (11)$$

The first point is exogenous parameter, i.e., it is not affected by the action, but it provides contextual information about the users' needs. Then, the other points provide the network state information, which are highly affected by the deployed configurations from the last action.

2) *Action*: We define the action for each agent k as all pairs of the reconfiguration control decisions (*sub-actions*) $i_k^n \in \mathcal{I}$, $x_k^n \in \mathcal{X}$, $y_k^n \in \mathcal{X}$, $z_k^n \in \mathcal{L}$, $\zeta_k^n \in \mathcal{M}$ and $p^n \in \mathcal{P}_k$. However, since the routing $p \in \mathcal{P}_k$ depends on the placement of the vDU and vCU, we can determine $p := \{p_{0m} \cup p_{ml} \cup p_{mk} \cup p_{lk}\} \in \mathcal{P}_k$ directly from i_k^n, z_k^n and ζ_k^n . For instance, if BS-5 with S1 decides $z_k^n := 1$ and $\hat{z}_k^n := 2$, then the selected path becomes $p := \{p_{0,2} \cup p_{2,1} \cup \emptyset \cup p_{1,5}\} \in \mathcal{P}_5$ with the transferred data flow EPC \rightarrow ES-2 \rightarrow FS-1 \rightarrow RU-5. Therefore, we can treat $p \in \mathcal{P}_k$ as part of the environment. Thus, we can formalize the action to be taken by each agent- k at each decision period n as a tuple:

$$a_k^n = \{i_k^n, x_k^n, y_k^n, z_k^n, \zeta_k^n\} \in \mathcal{A}_k, \quad \mathcal{A}_k = \mathcal{I} \times \mathcal{X} \times \mathcal{X} \times \mathcal{L} \times \mathcal{M}, \quad (12)$$

where \mathcal{A}_k is the action space of each agent- k , and we denote $a^n = \{a_k^n, \forall k \in \mathcal{K}\}$ as *the joint action* to be enforced to all the BSs. These action selections are trained from the LA and being enforced to each BS from the Near-RT RIC through the A1 interface.

3) *Reward & Policy*: We consider a non-cooperative setting, where each agent has its own reward function, i.e., $r_1^n(s_1^n, a_1^n), r_1^n(s_2^n, a_2^n), \dots, r_K^n(s_K^n, a_K^n)$. Thereby, we define the reward function at time slot n for each agent as:

$$r_k(a_k^n, s_k^n) := -J_k^n(a_k^n, s_k^n), \quad \forall k \in \mathcal{K}, \quad (13)$$

where $J_k^n(a_k^n, s_k^n)$ is the operation cost of each BS- k defined in Sec. II. By adopting IL, the optimal joint policy in (10) can be decomposed into the optimal policy per agent as:

$$\pi_k^* := \arg \max \mathbb{E}_{\pi_k} \left[\sum_{\tau=0}^{\infty} \gamma^\tau r_k^{\tau+n} | \pi_k \right], \quad \forall k \in \mathcal{K}, \quad (14)$$

where the policy of agent- k π_k is defined as a function that maps from its local state observation into action $\pi_k(s_k) : \mathcal{S}_k \mapsto \mathcal{A}_k, \forall k \in \mathcal{K}$, and $\mathbb{E}_{\pi_k} [\sum_{\tau=0}^{\infty} \gamma^\tau r_k^{\tau+n} | \pi_k], \forall k \in \mathcal{K}$ is the expected long-term accumulated reward of each agent- k starting at time slot τ . This MARL paradigm allows

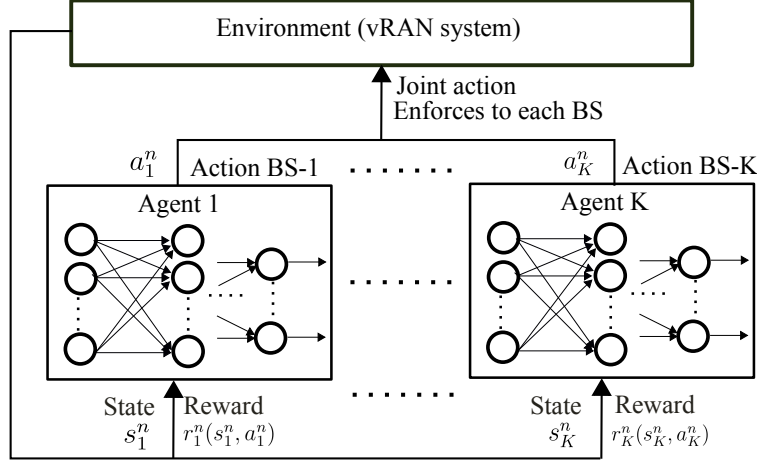


Fig. 6: LARV adopts model-free MARL with neural network architecture.

the number of possible actions to be reduced originally from $|\mathcal{A}_k|^K$ to $K \cdot |\mathcal{A}_k|$. Fig. 6 illustrates the architecture of MARL paradigm adopted by LARV.

B. Neural Network and Algorithm Design

After decomposing the joint policy in (10) using the MARL paradigm, we can focus on designing the optimal policy for each agent to maximize each agent's reward function as described in (14). However, finding the optimal policy of each agent is also non-trivial. First, each agent has a large state space, i.e., a continuous space from traffic demand. Then, even though the action space of each agent is discrete, it is large and multi-dimensional, comprising multiple control decisions (sub-actions), driving the combinatorial growth of the number of possible actions. In this case, traditional discrete action deep RL algorithms such as deep Q learning [32] become inefficient. To deal with such challenges, we deploy the BDQ architecture, a combination of an action branching architecture [25] and Dueling DDQN [26], for each agent's neural network. By applying BDQ, the multi-dimensions of the action can be distributed across individual network branches while maintaining a shared decision module among them to encode a latent representation of the input state and enable coordination among the branches. Furthermore, in contrast to traditional discrete-action deep RL algorithms, this decomposition of the actions exhibits a linear growth of the total network outputs with increasing action dimensionality. In [25], the branching architecture is initially applied to a problem where the size of each sub-action space is equal to each other, i.e., the discretization of the joint continuous action space. Here, we extend it to our vRAN problem, where the size of sub-action space also can be different. Fig. 7 illustrates the BDQ architecture adopted in each agent.

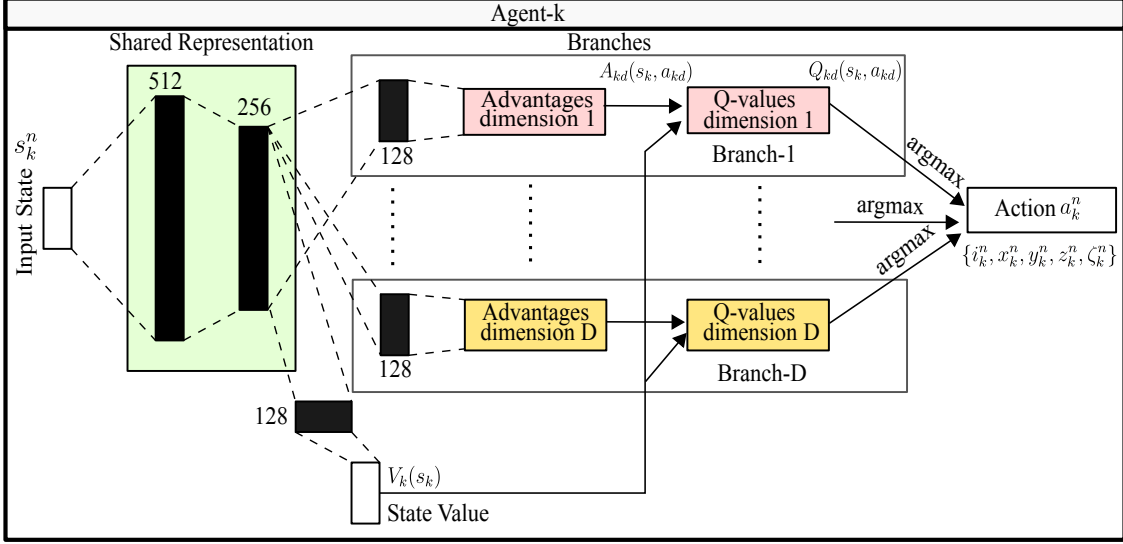


Fig. 7: The BDQ architecture applied at each agent.

1) *Dueling DDQN*: For each agent, the objective is to learn the optimal function $\pi_k^*(s_k) : S_k \mapsto \mathcal{A}_k, \forall k \in \mathcal{K}$. As the input state is a high-dimensional space and the output is a discrete action space, we use a neural network architecture to approximate the action-value function (Q-function) while the learning step is based on Double Q-learning.

We define the optimal action-value function $Q_k^*(s_k, a_k)$ for each agent- k as the maximum expected reward for observing certain sequences s_k after following some strategies π_k and taking some actions a_k as: $Q_k^*(s_k, a_k) := \max_{\pi} \mathbb{E}[\sum_{\tau} \gamma r_k^{\tau+n} | s_k^n = s_k, a_k^n = a_k]$. If we know the optimal value $Q_k^*(s'_k, a'_k)$ of the sequence at the next time slot s'_k for all possible action a'_k , we can identify the optimal strategy π_k^* , which is to select action a'_k that maximizes the expected value $r_k + \gamma Q_k^*(s'_k, a'_k)$: $Q_k^*(s_k, a_k) := \mathbb{E}_{s_k \sim \mathcal{E}} [r_k + \gamma \max_{a'_k} Q_k^*(s'_k, a'_k) | s'_k, a'_k]$. In the value iteration method, the action-value function can converge to the optimality when the iteration number reaches near infinity; however, it is impractical. Therefore, a function approximator such as a neural network can be applied to estimate the action-value function. The estimated action-value function parameterized by a neural network (Q-network) with weights θ is denoted as: $Q_k(s_k, a_k; \theta_k) \approx Q_k(s_k, a_k)$. Then, the Q-network is trained by minimization of a loss function:

$$L_k(\theta_k) := \mathbb{E}_{s_k, a_k, r_k, s'_k \sim \mathcal{D}_k} [u_k - Q_k(s_k, a_k; \theta_k)], \quad (15)$$

where the transition $\{s_k, a_k, r_k, s'_k\}$ is collected through random sampling (minibatches) from stored experience data \mathcal{D}_k , and u_k^i is the Temporal Difference (TD) target. In DQN [32], the TD

target is computed by:

$$u_k^{\text{DQN}} := \mathbb{E}_{s'_k \sim \mathcal{S}_k} [r_k + \gamma \max \tilde{Q}_k(s'_k, a'_k; \tilde{\theta}_k)], \quad (16)$$

where $\tilde{Q}_k(s'_k, a'_k; \tilde{\theta}_k)$ is the target network parameterized by weights $\tilde{\theta}_k$. However, the design of TD-target in (16) often causes an overestimate to the actual action-value. Thus, we apply DDQN [33] to overcome this issue by modifying the TD target to:

$$u_k^{\text{DDQN}} := \mathbb{E}_{s'_k \sim \mathcal{S}_k} [r_k + \gamma \tilde{Q}_k(s'_k, \arg \max_{a'_k} Q(s'_k, a'_k; \theta_k); \tilde{\theta}_k)]. \quad (17)$$

When the RL problem has a large action space such in our vRAN problem, it might not require estimating the value of all the action selections, i.e., avoiding unnecessary estimation of redundant and low-value actions. Thus, we apply the Dueling architecture [26] to DDQN by separating the Q-network into two streams of state-value and advantage, which are then combined through an aggregating layer to produce an estimate of the action-value function. Lets denote $V_k(s_k; \theta_k)$ and $A_k(s_k, a_k; \theta_k)$ as the estimated state-value function and advantage function, respectively; then, the action-value function at the output layer can be computed as:

$$Q_k(s_k, a_k; \theta_k) := V(s_k; \theta_k) + A_k(s_k, a_k; \theta_k) - \frac{1}{|\mathcal{A}|} \sum_{a'_k} A(s_k, a'_k; \theta_k). \quad (18)$$

The Dueling DDQN can recognize which one is the valuable state without learning the value of each action and can effectively achieve a high-quality policy for tackling a large state space. However, in addition to a large state space, our vRAN problem produces a multi-dimensional and huge discrete action space with combinatorial complexity at each agent. Next, we present how we incorporate an action branching architecture with Dueling DDQN to compress the action space at each agent in our vRAN problem.

2) *Action Space Compression with Action Branching*: Let us define a_{kd}^n as the d -th sub-action of agent- k at time slot n corresponds to the action set in (12), i.e., $a_{k1}^n := i_k^n, \dots, a_{kD}^n := \zeta_k^n, \forall k \in \mathcal{K}$, where $D := |a_k^n|$ is the number of action dimensions (branches). Then, the sub-action space for each agent- k can be represented as \mathcal{A}_{kd} , i.e., $\mathcal{A}_{k1} := \mathcal{I}, \dots, \mathcal{A}_{kD} := \mathcal{M}_k, \forall k \in \mathcal{K}$. As the action of each agent contains multiple sub-actions, the number of Q-values to be estimated for each agent turn to $\prod_{d=1}^D |\mathcal{A}_{kd}|$ in non-branching architectures. By incorporating action branching to Dueling DDQN (BDQ), the number of Q-values to be estimated can be compressed to $\sum_{d=1}^D |\mathcal{A}_{kd}|$.

Algorithm 1: LARV Operation

```

1 Initialize: Replay memory  $\mathcal{D}_k, \forall k$  with a fixed buffer size, BDQ-network  $Q_{\theta_k}, \forall k$  with
   random or pretraining weights  $\theta_k$ .
2 Clone BDQ-network to target network  $\tilde{Q}_{\tilde{\theta}_k}$  with weights  $\tilde{\theta}_k \leftarrow \theta_k, \forall k$ .
3 for Each episode  $e = 1.., E$  do
4   Reset state of each BS  $s_k^1 = \{\lambda^1, 1, x_k^{\max}, \hat{x}_k^{\max}, 0, 0, 0\}, \forall k \in \mathcal{K}$ .
5   for Each time slot  $n = 1.., N$  do
6     Select random action  $a_k^n, \forall k \in \mathcal{K}$  with probability  $\epsilon$ , otherwise compute
        $a_k^n, \forall k \in \mathcal{K}$  by using (22).
7     Determine the routing  $p \in \mathcal{P}_k, \forall k \in \mathcal{K}$  using  $i_k^n, z_k^n$  and  $\zeta_k^n$  obtained from  $a_k^n$ .
8     Enforce  $a_k^n$  and  $p \in \mathcal{P}_k$  to each BS and compute the cost  $J_k^n, \forall k \in \mathcal{K}$ .
9     Collect the reward for each agent  $r_k^n, \forall k \in \mathcal{K}$  based on (13).
10    Set the next state  $s_k^{n+1} \leftarrow s_k^n, \forall k \in \mathcal{K}$ .
11    Store the experience  $\mathcal{D}_k \leftarrow \{s_k^n, a_k^n, r_k^n, s_k^{n+1}\}, \forall k \in \mathcal{K}$ .
12    Sample random minibatch of experiences from  $\mathcal{D}_k, \forall k \in \mathcal{K}$ .
13    Compute TD target  $u_k^{\text{BDQ}}, \forall k \in \mathcal{K}$  using (20).
14    Perform a gradient descent on  $L_k(\theta_k), \forall k \in \mathcal{K}$  w.r.t  $\theta_k$  from (21).
15    Update target network  $\hat{Q}_{\hat{\theta}_k} \leftarrow Q_{\theta_k}, \forall k \in \mathcal{K}$  for every  $C$  steps.
16  end
17 end

```

In BDQ, we use a common state s_k and state-value $V_k(s_k)$ for each agent- k . Hence, the value of sub-action a_{kd} at state s_k with the corresponding sub-action advantages $A_{kd}(s_k, a_{kd})$ becomes:

$$Q_{kd}(s_k, a_{kd}) := V_k(s_k) + (A_{kd}(s_k, a_{kd}) - \frac{1}{|\mathcal{A}_{kd}|} \sum_{a'_{kd} \in \mathcal{A}_{kd}} A_{kd}(s_k, a'_{kd})). \quad (19)$$

The TD target in BDQ is set similar to (17) to avoid maximization bias, except it uses an average of all the dimensions of the action as follows:

$$u_k^{\text{BDQ}} := r_k + \gamma \frac{1}{D} \sum_d \tilde{Q}_{kd}(s'_k, \arg \max_{a'_{kd} \in \mathcal{A}_{kd}} Q_{kd}(s'_k, a'_{kd})), \quad (20)$$

where \tilde{Q}_{kd} is the target network. Then, the loss function can be computed as:

$$L_k(\theta_k) := \mathbb{E}_{s_k, a_k, r_k, s'_k \sim \mathcal{D}} \left[\frac{1}{D} \sum_d [u_k^{\text{BDQ}} - Q_{kd}(s_k, a_{kd}; \theta_k)] \right]. \quad (21)$$

The action to be taken for each BS is selected based on ϵ -greedy strategy, where each agent chooses a random action with probability ϵ or compute:

$$a_k := \left[\arg \max_{a'_{k1}} Q_{k1}(s_k, a_{k1'}), \dots, \arg \max_{a'_{kD}} Q_{kD}(s_k, a_{kD'}) \right] \quad (22)$$

with probability $1 - \epsilon$. Algorithm 1 summarizes the LARV training process incorporating MARL paradigm with BDQ architecture.

IV. RESULTS AND DISCUSSION

In this section, we perform trace-driven simulations using real traces collected from our testbed to evaluate the performance of LARV under various scenarios during the training process and online operation. We also use the following policies as benchmarks.

- *The best static with 100% provisioning (BSP)*: It knows exactly the peak future traffic demand of each BS and utilizes them to find the best static joint action via an exhaustive search. It can be defined as: $\pi_{BSP} := \arg \min_a \sum_k^K J_k^i(a)$, where $i = \arg \max_n \lambda_k^n$. Further, it is used to normalized the monetary costs in the online operation evaluations.
- *The best static with hindsight (BHS)*: It has access to an oracle of traffic demands $\{\lambda_k^n\}_{n=1}^N, \forall k \in \mathcal{K}$ (and system parameters). The solution, which is the best static joint action that minimizes the long-term total cost, can only be designed in hindsight. It is defined as $\pi_{BHS} := \arg \min_a \sum_{n=1}^N \sum_{k=1}^K J_k^n(a)$. It is unfeasible in practice as assuming an oracle of the traffic demands (and system parameters) are unrealistic.
- *Fully multi-agent of Dueling DDQN (MDQ)*: It is a non-branching Dueling DDQN solution. In every BS, each reconfiguration control works as a separate agent that takes an independent decision, i.e., the decision of each split, resource, and location is controlled by a different agent. Each agent adopts Dueling DDQN and shares the common state and reward if only the control decisions are in the same BS. It is an adaptive policy and the closest deep RL benchmark to LARV.

A. Experimental Setup

We built a bespoke testbed to collect measurements used to evaluate LARV under realistic conditions. We utilize the software-based srsRAN [24], where each entity is virtualized using container-based virtualization from Docker. The radio interfaces of the BS (e.g., RU) and user are emulated via ZMQ. The srsENB acts as a BBU of the BS. We deploy the virtualized entities in Platform A (CSC cPouta hpc.5.16core with max. 16 vCPU) and Platform B (PC AMD Ryzen 7 PRO 4750U with max. 16 CPU threads). We use these computing specifications for *Reference Core (RC)*, i.e., 1 RC translates to 1 CPU thread and 1 vCPU. The virtualized resource of each container can be controlled through `-cpus`, which allows us to set a capacity limit and isolate each container resource. We set an initial resource reservation for srsENB with 10 RCs. In our

measurements, the traffic demand follows a Poisson-generated user datagram protocol with a peak data rate is 36.6 Mbps (SISO 10 MHz LTE).

In our simulations, the traffic demands follow the Milan network datasets from Telecom Italia [12] with 10 minutes time interval. Considering the limitations of our testbed and the difficulty in capturing the computing behavior of the Milan traffic in a tractable model, we utilize a deep neural network⁷ to map the Milan traffic demands into the actual resource utilization, trained using our collected measurements. The computing consumptions of LP, HP, LM, HM, LR, HR, and PD functions yield 48%, 17%, 7%, 7%, 0.5%, 0.5%, 10%, 10% of the total BBU, respectively, cf. [13], [14]. We consider a realistic MEC-based Milan topology (N1) [35] and a synthetic topology (N2) generated using the Waxman algorithm [36]. N2 has parameters of link probability (0.5) and edge length control (0.1). A vRAN system in N1 and N2 consists of 1 EPC, 4 ESs, 8 FSs and 8 RUs (default), where the routers are co-located with each node. Per link's latency, capacity, and weights of N1 and N2 vary from 0 to 0.1 ms, 30 Gbps to 160 Gbps, and 0 to 0.1. We have $H_l = 50$ RCs, $\forall l \in \mathcal{L}$ and $\hat{H}_m = 200$ RCs, $\forall m \in \mathcal{M}$. We set the available flavors with $|\mathcal{X}| = 16$ for Platform A and Platform B, which translates to $\{0, 1, \dots, 14, 15\}$ RCs of the computing resources. Then, we define two vRAN systems in which we utilize Platform A with N1 (VR1) and Platform B with N2 (VR2).

We set the default coefficient fees with $\kappa_O := 1$, $\kappa_D := 5$, $\kappa_I := \kappa_R := 0.5$, $\kappa_{RU} := 1$ and $\kappa_H := 1$. Considering computational processing cost is less by centralizing more functions and executing them in a higher computing platform, we set $\kappa_{FS} := 0.5\kappa_{RU}$ and $\kappa_{ES} := 0.5\kappa_{FS}$ (c.f. [37, Fig. 6a] with ≈ 10 BSs). Then, each agent has a BDQ-network consisting of D branches, where it has a shared input with size of $|s_k|$. Each d -th branch has an output with size of $|\mathcal{A}_{kd}|$. The hidden layers of BDQ are constructed from fully connected linear layers activated by ReLU function, where the size of each layer can be seen in Fig. 7. The target network is updated every 1000 time slots. The batch size is set with 128 and the replay buffer has a capacity of 10^6 . Our exploration and exploitation strategy is based on ϵ -greedy, where we set $\epsilon_{\max} = 1$ at the beginning of episode, then it exponentially decays to $\epsilon_{\min} = 0.015$. We use Adam optimizer [34] with learning rate is set to 0.0001 and (21) for the loss function. The default time horizon is one day (144 time slots) during the training process and we use the next two days (288 time

⁷It is constructed from an input, an output and three hidden layers with the sizes of 128, 64 and 16. We use Adam optimizer [34] with learning rate is set to 5×10^{-5} , mini-batch with the size of 128 and MSE loss function, then train it with 200 epochs.

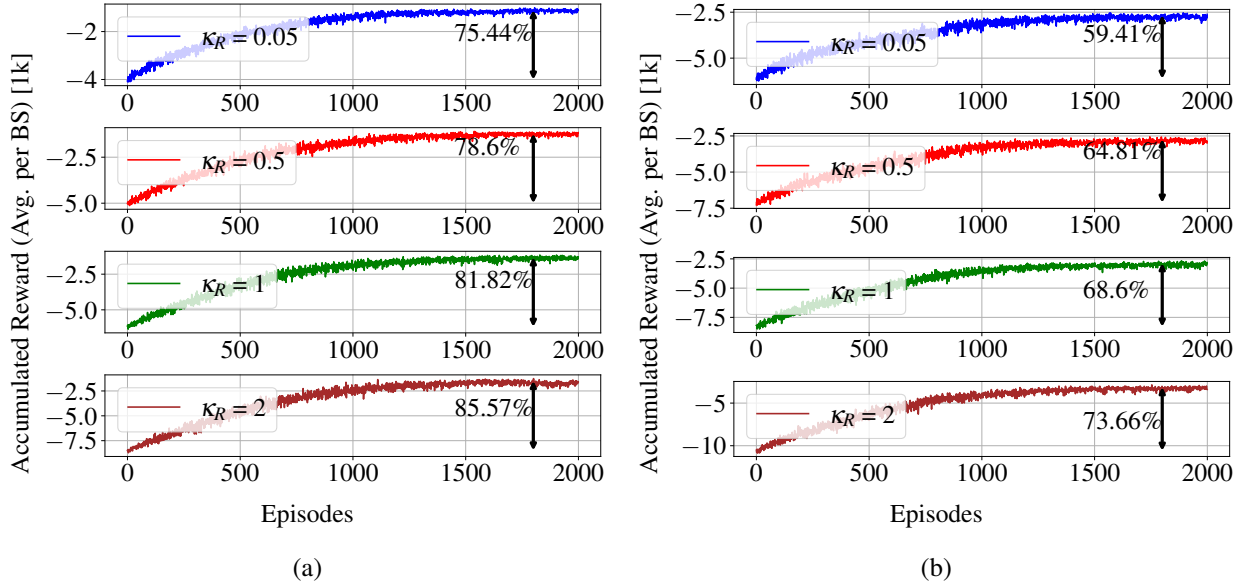


Fig. 8: The convergence of LARV under various reconfiguration fees in a) VR1 and b) VR2.

slots) for the online operation. Finally, we plan to release our datasets in this work online.

B. Performance during Training Process

1) *Training Convergence*: Fig. 8 illustrates the convergence behavior of LARV over various reconfiguration coefficient fees in VR1 and VR2. At the beginning of episodes, LARV has a higher probability of utilizing a random policy for exploration. As a result, LARV produces a significant long-term total operation cost over all the reconfiguration fees in VR1 and VR2. However, after some episodes, LARV successfully learns the optimal policy and converges to the best policy the agents can learn. Moreover, we found a similar trend in LARV’s behavior, where it manages to converge to some cost values after 1500 episodes, albeit it learns over different reconfiguration fees and vRAN systems.

Fig. 8 also shows that using a random policy in vRAN reconfiguration problem must be avoided as it yields in costly long-term cost. In VR1, our findings reveal that LARV can save the costs by up to 75.44%, 78.6%, 81.82% and 85.57% over $\kappa_R = 0.05$, $\kappa_R = 0.5$, $\kappa_R = 1$ and $\kappa_R = 2$, respectively, compared to a random policy. Such significant cost savings by LARV also appear in VR2, where LARV can save the cost as high as 75.66% ($\kappa_R = 5$). The cost savings of LARV also increase when the reconfiguration fee is more expensive (e.g., $\kappa_R = 0.05$ to $\kappa_R = 2$), where it grows from 75.44% to 85.57% in VR1 and from 59.41% to 73.66% in VR2.

2) *Declined Demands*: Fig 9 shows that LARV can reduce the incurred cost due to declined demands after several training episodes both in VR1 and VR2. The declined demand cost appears

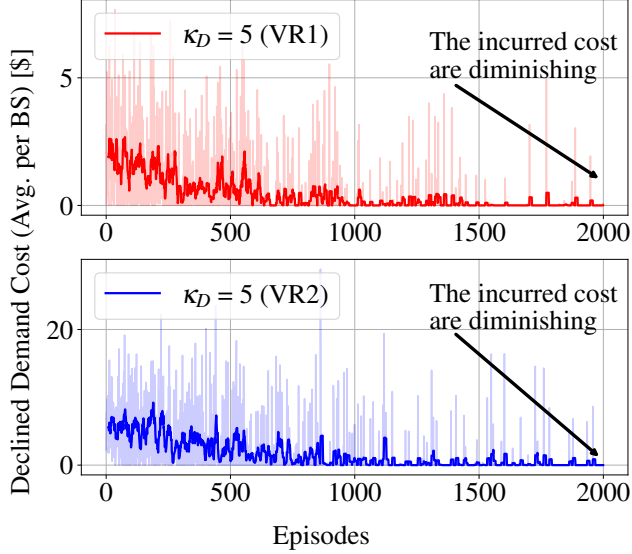


Fig. 9: The incurred cost from declined service demands (average per BS) in VR1 and VR2. The cost is diminishing as the training goes, and it eventually reaches to near zero (e.g., after 1900 episodes).

almost every episode when the training does not reach 1000 episodes. The main reason is that LARV mostly chooses random actions for exploration, rendering a very high number of declined service demands and, at the same time, producing a very expensive cost. As the training goes, LARV optimizes its weights based on the reward feedback (e.g., the declined demands render a significantly more expensive cost) and successfully diminishes the declined demand cost. After 1000 episodes, the incurred cost at each episode becomes smaller and less frequent, then this cost eventually reaches almost zero (or zero) after 1900 episodes. Following the decrease of this cost, at the same time, the accumulated total operation cost (see Fig. 8) is also greatly diminished.

3) *Transfer Learning*: To assess the generalization of LARV over heterogeneous vRAN systems, we study the benefits of utilizing a transfer learning paradigm (“w/ transfer”) compared to learning from scratch (“w/o transfer”). In particular, we leverage our pre-trained neural network weights (trained in VR1) for initializing the other neural network weights in different vRAN systems (e.g., in VR2). It is worth noting that the system parameters and platforms in VR1 and VR2 are different. Hence, this evaluation aim to study the possibility of reusing the existing models for the other vRAN systems, which might expedite the convergence and widespread deployment of LARV. We use the same default hyperparameter (defined in Sec. IV-A), except we encourage less exploration for “w/ transfer” by modifying $\epsilon_{\max} = 1$ to $\epsilon_{\max} = 0.1$.

Fig. 10 depicts that LARV “w/ transfer” successfully converges to the similar value with “w/o transfer” in VR2, albeit the pre-trained weights are leveraged from a different vRAN system

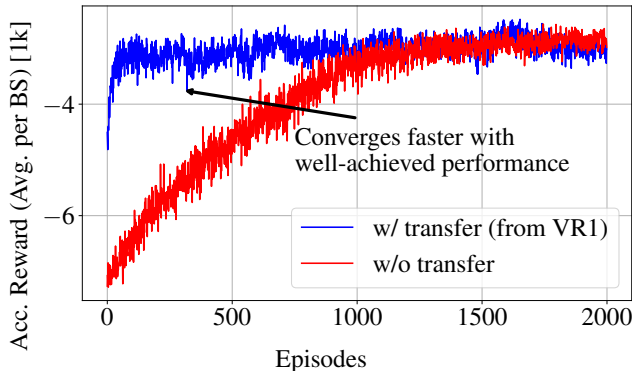


Fig. 10: Training convergence in VR2. Using transfer learning paradigm (“w/ transfer”), which is leveraged from pretraining weights in VR1, can achieve similar performance and faster convergence compared to without transfer learning (“w/o transfer”).

(VR1). Moreover, “w/ transfer” can speed up the training convergence, where it starts to converge after around 150 episodes. Therefore, using a transfer learning paradigm, LARV offers a faster learning convergence and, simultaneously, the possibility to reuse existing pre-trained models across different vRAN systems, with similar performance as “w/o transfer” even though the pre-training is conducted not in the same platform.

4) *Action Space Compression*: Following the simulation setup, each BS in VR1 and VR2 has sub-action sizes with $|\mathcal{I}|=4$, $|\mathcal{X}|=16$, $|\mathcal{L}|=8$ and $|\mathcal{M}|=4$. Hence, the number of Q values to be estimated is around 3.2×10^4 for each BS and becomes 1.32×10^{36} for all the BSs. LARV turns such a combinatorial growth into a linear increase; hence, the estimated Q values become 48 for each BS and 384 for all the BSs.

C. Performance during Online Operation

1) *Duration of Online Operation*: Fig. 11a visualizes the performance of LARV compared to the benchmarks over various time horizon settings, ranging from 2 days to 10 days. We found that LARV becomes the most cost-effective approach by having the cheapest long-term total cost. The performance of LARV also remains stable, albeit in varying conditions (demands and resource availability). Compared to the best static policy with provisioning (BSP) and hindsight (BHS), the cost-savings of LARV can be as high as 36% and 26%, respectively. Hence, these savings clearly emphasize the importance of updating the vRAN configurations to adapt to the varying conditions. Moreover, LARV also outperforms MDQ, where it saves the long-term total cost by up to 25%. This gain shows the effectiveness of LARV in solving the vRAN reconfiguration problem compared to a non-branching state-of-the-art deep RL approach.

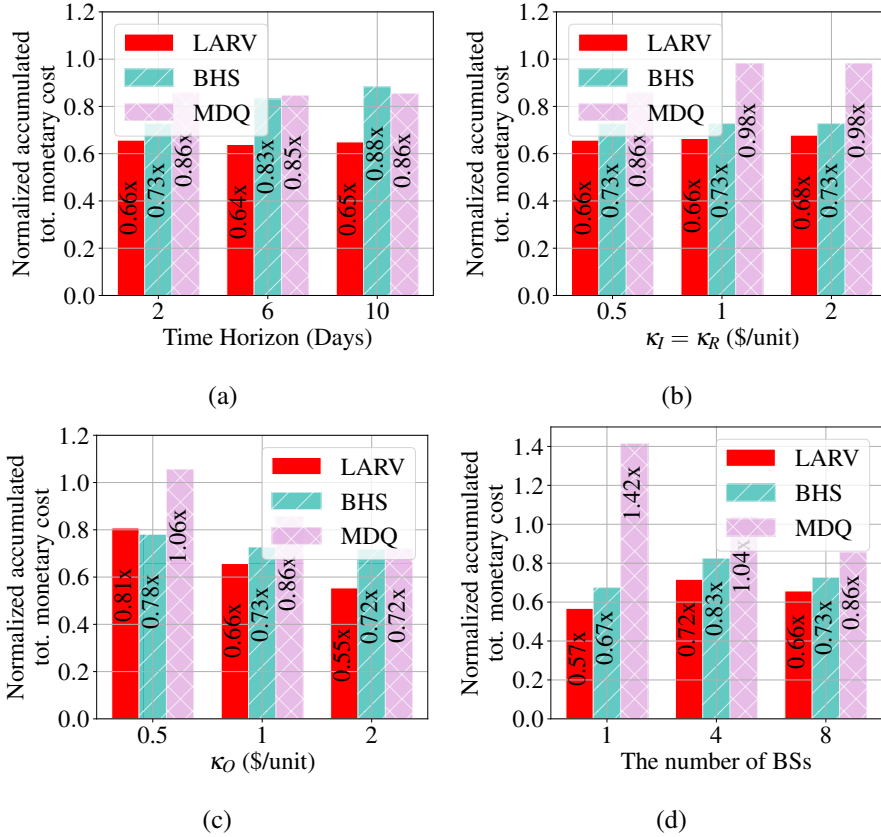


Fig. 11: Performance during the online operation in VR1. The presented monetary costs are normalized to BSP.

2) *Reconfiguration fees:* We analyze the impact of various reconfiguration coefficient fees on the cost savings that LARV can achieve. Fig. 11b shows that LARV can successfully provide well-achieve performance in both cheap and expensive reconfiguration fees. It also shows that the increase in reconfiguration fee slightly affects the performance of LARV while it significantly degrades MDQ. Note that BSP and BHS are not affected by the reconfiguration fee as they are a static policy. Moreover, by reducing $\kappa_R = 2$ to $\kappa_R = 0.5$, the cost savings of LARV increase from 32% to 34% and 7% to 10% compared to BSP and BHS, respectively. These findings emphasize that reconfiguring the vRAN system is beneficial, particularly when the reconfiguration fee is affordable. Moreover, LARV also reduces the cost of MDQ by up to 33% ($\kappa_R = 1$), and this underlines that we need to carefully design the deep RL algorithm for the vRAN reconfiguration problem to deliver better cost-efficient vRAN long-term operations.

3) *Overprovisioning fees:* We study the effect of different overprovisioning coefficient fees to the performance of LARV. As seen from Fig. 11c, LARV generally outperforms BSP, BHS and MDQ, where it is just slightly more expensive (around 3%) than BHS in terms of a low

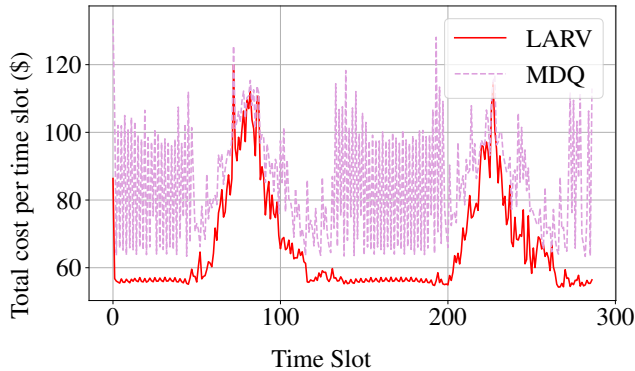


Fig. 12: The incurred total cost at each time slot.

overprovisioning fee ($\kappa_0 = 0.5$). Importantly, LARV becomes more cost-effective than the static policy benchmarks when overprovisioning fee is higher (e.g., more valuable resources). It is shown by the cost savings of LARV that increase from 19% to 45% and from -3% to 24% compared to BSP and BHS, respectively. However, compared to MDQ, the cost savings of LARV remain stable, where it gains around 24% throughout various overprovisioning fees. These findings highlight the need for reconfiguring the vRAN system at runtime, particularly when the resources are valuable and the price of wasting such resources is high, making the static policy approaches economically unviable for long-term operations.

4) *The Number of BSs:* We evaluate LARV over a different number of the BSs in a vRAN system. The number of agents adopted by LARV and MDQ equals the number of BSs. Fig. 11d illustrates that LARV is the most cost-efficient approach compared to the other benchmarks, albeit the number of BSs varies. We also found that the highest cost reduction by LARV can be found when there is only a single BS. For example, when $K = 1$, LARV can save the cost by up to 43%, 15% and 59% of BSP, BHS and MDQ, respectively. These findings show that LARV can perform best with a single BS (no competing agent). However, it is not limited and easily adjusted to the other number of the BSs without significantly degrading its performance.

5) *The Incurred Total Cost per Slot:* Fig. 11d illustrate the incurred total cost at every time slot by LARV and MDQ in BS-1. Both approaches are adaptive, and they can reconfigure the system at each time slot. As seen in Fig. 11d, LARV produces a cheaper total cost almost at every time slot. This advantage becomes more significant when the traffic demand is low, i.e., at the time slots 1 to 50 and 125-200. Therefore, LARV also can obtain considerable cost savings for long-term operation compared to MDQ.

V. CONCLUSION

In this paper, we have proposed LARV that jointly reconfigures the functional splits of the BSs, the resources and placements of vDUs and vCUs, and the routing for each BS flow. The objective of LARV is to minimize the long-term total operation cost while adapting to the possibly-varying traffic demands and resource availability. In particular, we have analyzed the relations between the traffic demands and resource utilization in the vRAN system, which renders their relations have high variance and dependence on platform and platform load. We also have formulated a comprehensive cost model capturing the impacts of resource overprovisioning, instantiation and reconfiguration and the declined demands. We have developed LARV using a model-free MARL paradigm to solve the sequential decision-making problem, where each agent's neural network is developed using the BDQ architecture, and they learn the optimal policy to select the actions that reconfigure the BSs through IL. We also have conducted a series of trace-driven evaluations during the training process and online operation. The numerical results have shown that LARV successfully learns the optimal policy and can be readily applied to different vRAN systems via transfer learning with similar performance and faster convergence compared to non-transferred learning. Moreover, LARV offers considerable cost savings by up to 45% of the static benchmarks and 33% of a non-branching Dueling DDQN solution.

REFERENCES

- [1] L. Bonati *et al.*, "Open, Programmable, and Virtualized 5G Networks: State-of-the-Art and the Road Ahead," *Computer Networks*, vol. 182, p. 107516, 2020.
- [2] "5G immersive service opportunities with Edge Cloud and Cloud RAN (White Paper)," Nokia, Tech. Rep., 2019.
- [3] "Nokia Mobile Anyhaul (White Paper)," Nokia, Tech. Rep., 2017.
- [4] "Open and Virtualized - The Future Radio Access Network," NEC, Tech. Rep., 01 2020.
- [5] "O-RAN-WG1-O-RAN Architecture Description v01.00.00," O-RAN Alliance, Technical Specification (TS), 02 2020.
- [6] 3GPP, "Architecture description (Release 16)," 3rd Generation Partnership Project (3GPP), Technical Specification Group Radio Access Network (NG-RAN) 38.401, 03 2020, version 16.1.0.
- [7] F. W. Murti, J. A. Ayala-Romero, A. Garcia-Saavedra, X. Costa-Pérez, and G. Iosifidis, "An Optimal Deployment Framework for Multi-Cloud Virtualized Radio Access Networks," *IEEE Transactions on Wireless Communications*, vol. 20, no. 4, pp. 2251–2265, 2021.
- [8] G. Paschos *et al.*, "Wireless caching: technical misconceptions and business barriers," *IEEE Communications Magazine*, vol. 54, no. 8, pp. 16–22, 2016.
- [9] A. M. Alba, J. H. G. Velásquez, and W. Kellerer, "An adaptive functional split in 5G networks," in *IEEE INFOCOM 2019 - IEEE Conference on Computer Communications Workshops (INFOCOM WKSHPS)*, 2019, pp. 410–416.
- [10] J. A. Ayala-Romero *et al.*, "vrAI: Deep Learning based Orchestration for Computing and Radio Resources in vRANs," *IEEE Transactions on Mobile Computing*, pp. 1–1, 2020.
- [11] J. A. Ayala-Romero, A. Garcia-Saavedra, X. Costa-Perez, and G. Iosifidis, "Orchestrating energy-efficient vrans: Bayesian learning and experimental results," *IEEE Transactions on Mobile Computing*, pp. 1–1, 2021.
- [12] T. Italia, "Telecommunications - SMS, Call, Internet - MI," 2015. [Online]. Available: <https://doi.org/10.7910/DVN/EGZHfV>

- [13] A. Garcia-Saavedra *et al.*, “Joint Optimization of Edge Computing Architectures and Radio Access Networks,” *IEEE Journal on Selected Areas in Communications*, vol. 36, no. 11, 2018.
- [14] F. Z. Morais *et al.*, “PlaceRAN: optimal placement of virtualized network functions in Beyond 5G radio access networks,” *IEEE Transactions on Mobile Computing*, pp. 1–1, 2022.
- [15] A. M. Alba, S. Janardhanan, and W. Kellerer, “Enabling Dynamically Centralized RAN Architectures in 5G and Beyond,” *IEEE Transactions on Network and Service Management*, vol. 18, no. 3, pp. 3509–3526, 2021.
- [16] A. M. Alba and W. Kellerer, “Dynamic Functional Split Adaptation in Next-Generation Radio Access Networks,” *IEEE Transactions on Network and Service Management*, 2022.
- [17] D. Harutyunyan and R. Riggio, “Flex5G: Flexible Functional Split in 5G Networks,” *IEEE Transactions on Network and Service Management*, vol. 15, no. 3, pp. 961–975, 2018.
- [18] S. Ali *et al.*, “6G White Paper on Machine Learning in Wireless Communication Networks,” 2020.
- [19] F. W. Murti, S. Ali, and M. Latva-aho, “Constrained Deep Reinforcement Based Functional Split Optimization in Virtualized RANs,” *IEEE Transactions on Wireless Communications*, 2022.
- [20] T. Pamuklu, M. Erol-Kantarci, and C. Ersoy, “Reinforcement Learning Based Dynamic Function Splitting in Disaggregated Green Open RANs,” in *ICC 2021 - IEEE International Conference on Communications*, 2021, pp. 1–6.
- [21] L. Bonati, S. D’Oro, M. Polese, S. Basagni, and T. Melodia, “Intelligence and Learning in O-RAN for Data-Driven NextG Cellular Networks,” *IEEE Communications Magazine*, vol. 59, no. 10, pp. 21–27, 2021.
- [22] M. Polese, L. Bonati, S. D’Oro, S. Basagni, and T. Melodia, “CoIO-RAN: Developing Machine Learning-based xApps for Open RAN Closed-loop Control on Programmable Experimental Platforms,” *IEEE Transactions on Mobile Computing*, pp. 1–14, 2022.
- [23] F. W. Murti, S. Ali, G. Iosifidis, and M. Latva-Aho, “Learning-Based Orchestration for Dynamic Functional Split and Resource Allocation in vRANs,” in *2022 Joint European Conference on Networks and Communications & 6G Summit (EuCNC/6G Summit)*, 2022, pp. 243–248.
- [24] I. Gomez-Miguel *et al.*, “SrsLTE: An Open-Source Platform for LTE Evolution and Experimentation,” in *Proceedings of the Tenth ACM International Workshop on Wireless Network Testbeds, Experimental Evaluation, and Characterization*, 2016, p. 25–32.
- [25] A. Tavakoli, F. Pardo, and P. Kormushev, “Action Branching Architectures for Deep Reinforcement Learning,” in *AAAI Conference on Artificial Intelligence*, 2018, pp. 4131–4138.
- [26] Z. Wang, T. Schaul, M. Hessel, H. Van Hasselt, M. Lanctot, and N. De Freitas, “Dueling network architectures for deep reinforcement learning,” ser. ICML’16. JMLR.org, 2016, p. 1995–2003.
- [27] J. Y. Yen, “Finding the K Shortest Loopless Paths in a Network,” *Management Science*, vol. 17, no. 11, 1971.
- [28] D. Bega, M. Gramaglia, M. Fiore, A. Banchs, and X. Costa-Perez, “AZTEC: Anticipatory Capacity Allocation for Zero-Touch Network Slicing,” in *IEEE INFOCOM 2020 - IEEE Conference on Computer Communications*, 2020, pp. 794–803.
- [29] 5G-CORAL, “Refined design of 5G-CORAL orchestration and control system and future directions,” Public Deliverable D3.2, May 2019.
- [30] L. Matignon, G. j. Laurent, and N. Le fort piat, “Review: Independent reinforcement learners in cooperative markov games: A survey regarding coordination problems,” *Knowl. Eng. Rev.*, vol. 27, no. 1, p. 1–31, feb 2012.
- [31] A. Neyman, “From markov chains to stochastic games,” in *Stochastic Games and Applications*, A. Neyman and S. Sorin, Eds. Dordrecht: Springer Netherlands, 2003, pp. 9–25.
- [32] V. Mnih *et al.*, “Human-level control through deep reinforcement learning,” *Nature*, vol. 518, 2015.
- [33] H. v. Hasselt, A. Guez, and D. Silver, “Deep reinforcement learning with double q-learning,” ser. AAAI’16. AAAI Press, 2016, p. 2094–2100.
- [34] D. P. Kingma and J. Ba, “Adam: A method for stochastic optimization,” in *3rd International Conference on Learning Representations, ICLR 2015*, 2015.
- [35] B. Xiang, J. Elias, F. Martignon, and E. Di Nitto, “A dataset for mobile edge computing network topologies,” *Data in Brief*, vol. 39, p. 107557, 2021.
- [36] B. Waxman, “Routing of multipoint connections,” *IEEE Journal on Selected Areas in Communications*, vol. 6, no. 9, pp. 1617–1622, 1988.
- [37] P. Rost, S. Talarico, and M. C. Valenti, “The complexity–rate tradeoff of centralized radio access networks,” *IEEE Transactions on Wireless Communications*, vol. 14, no. 11, pp. 6164–6176, 2015.